HHS Public Access

Author manuscript

Biopolymers. Author manuscript; available in PMC 2021 October 26.

Published in final edited form as:

Biopolymers. 2021 October ; 112(10): e23402. doi:10.1002/bip.23402.

Specific binding-induced modulation of the XCL1 metamorphic equilibrium

Acacia F. Dishman[1,2], **Francis C. Peterson**[1], **Brian F. Volkman**[1]

[1]Department of Biochemistry, Medical College of Wisconsin, Milwaukee, Wisconsin, USA

[2]Medical Scientist Training Program, Medical College of Wisconsin, Milwaukee, Wisconsin, USA

Abstract

The metamorphic protein XCL1 switches between two distinct native structures with different functions in the human immune system. This structural interconversion requires complete rearrangement of all hydrogen bonding networks, yet fold-switching occurs spontaneously and reversibly in solution. One structure occupies the canonical α-β chemokine fold and binds XCL1's cognate G-protein coupled receptor, while the other structure occupies a dimeric, all-β fold that binds glycosaminoglycans and has antimicrobial activity. Both of these functions are important for the biologic role of XCL1 in the immune system, and each structure is approximately equally populated under near-physiologic conditions. Recent work has begun to illuminate XCL1's role in combatting infection and cancer. However, without a way to control XCL1's dynamic structural interconversion, it is difficult to study the role of XCL1 fold-switching in human health and disease. Thus, a molecular tool that can regulate the fractional population of the two XCL1 structures is needed. Here, we find by heparin affinity chromatography and NMR that an engineered XCL1 variant called CC5 can trigger a dose-dependent shift in XCL1's metamorphic equilibrium such that the receptor binding structure is depleted, and the antimicrobial structure is more heavily populated. This shift likely occurs due to formation of XCL1-CC5 heterodimers in which both protomers occupy the β-sheet structure. These findings lay the groundwork for future studies seeking to understand the functional role of XCL1 metamorphosis, as well as studies screening for a drug-like molecule that can therapeutically target XCL1 by tuning its metamorphic equilibrium. Moreover, the proof of concept presented here suggests that protein metamorphosis is druggable, opening numerous avenues for controlling biological function of metamorphic proteins by altering the population of their multiple native states.

Correspondence: Brian F. Volkman, Department of Biochemistry, Medical College of Wisconsin, Milwaukee, WI, USA. bvolkman@mcw.edu.

AUTHOR CONTRIBUTIONS

Acacia F. Dishman and Brian F. Volkman conceived and planned experiments. Acacia F. Dishman produced and purified proteins, performed heparin affinity chromatography experiments and HSQC experiments, and analyzed data. Francis C. Peterson performed HSQC experiments. Acacia F. Dishman prepared manuscript figures and wrote the first manuscript draft. Francis C. Peterson and Brian F. Volkman assisted in manuscript writing and revision.

CONFLICT OF INTEREST

Francis C. Peterson and Brian F. Volkman have ownership interests in Protein Foundry, LLC.

DATA AVAILABILITY STATEMENT

Data available on request from the authors

SUPPORTING INFORMATION

Additional supporting information may be found online in the Supporting Information section at the end of this article.

Keywords

chemokine; metamorphic protein; NMR; XCL1

1 | INTRODUCTION

Metamorphic proteins defy the canonical protein folding paradigm to adopt multiple, incompatible structures.[1–3] The human chemokine XCL1 is a metamorphic protein that exists as a mixture of two equally populated native state conformations under near-physiologic conditions.[4] XCL1 interconverts spontaneously and reversibly between its two structures,[4] which are (1) the canonical α − β chemokine fold, and (2) a 4-stranded β-sheet that forms a dimer (Figure 1A).[5,6] Fold 1 binds to XCL1's receptor, XCR1 and Fold 2 binds to glycosaminoglycans (GAGs) and has antimicrobial activity (Figure 1B).[4,7,8] Chemokines other than XCL1 bind their cognate receptors and GAGs using one structure. XCL1, however, requires both its folds to carry out these two essential functions, enabling XCL1 to perform its roles in the cytotoxic immune response[9–11] and thymic establishment of self-tolerance.[10,12] Emerging evidence demonstrates that XCL1 plays a role in fighting infection[7,8,13–15] and cancer.[16–19] However, it is difficult to study the biologic role of XCL1 metamorphosis due to XCL1's constant, dynamic structural interconversion.

Studying XCL1 metamorphosis is further complicated by the fact that changes in certain environmental conditions have been found to shift XCL1's structural equilibrium.[4,6] Under high sodium chloride concentrations and low temperatures, XCL1 prefers the chemokine fold, while under low sodium chloride concentrations and high temperatures, XCL1 prefers the β-sheet fold.[4,6] Under near-physiologic conditions (150 mM NaCl, 37 °C), XCL1 occupies each structure in near-equal proportion.[4] It is also known that the presence of the glycosaminoglycan heparin causes an increase in the fractional population of XCL1's β-sheet structure.[4] However, heparin, heparan sulfate, and other GAG oligomers are poor candidates for manipulating XCL1's metamorphic equilibrium because they are nonspecific binding partners for most chemokines and many other cytokines and extracellular proteins. Binding of the heparin oligosaccharides also causes XCL1 to precipitate out of solution.[4]

To aid in parsing out the biologic roles of the two XCL1 structures, variants of XCL1 that lock it into each of its native conformations have been designed.[14,20] CC3 is an engineered XCL1 variant that is locked into the chemokine structure by the addition of a disulfide staple between the α-helix and the N-loop.[20] Likewise, the engineered XCL1 variant CC5 is locked into the β-sheet structure by the addition of an intramolecular disulfide staple between the β2 and β3 strands.[14] In other words, the CC5 staple is within one monomeric subunit of the β-sheet homodimer, not between dimer subunits. In addition to locking XCL1 into each structure with disulfide staples, it would be valuable to control the fractional population of the XCL1 structures where wild type XCL1 is already present, for example, in tissue culture and *in vivo* experiments. An XCL1-specific ligand that can shift its structural equilibrium in solution would be useful for biochemical and biomedical studies requiring real-time control of the relative population of the XCL1 structures in the presence of constant temperature and salt conditions (e.g., physiologic solution conditions).

Here, we show that the engineered XCL1 variant CC5 can control XCL1's structural equilibrium. Many metamorphic proteins form protein-protein interfaces that stabilize one of their structures relative to the other, such as Selecase, RfaH, and XCL1.[6,21,22] In the case of XCL1, the interface is formed between two subunits of a homodimer.[6] We hypothesized that when CC5 is titrated into XCL1, the excess β-sheet-stabilizing subunits would shift the metamorphic equilibrium by dimerizing with wild-type XCL1 molecules in the β-sheet conformation (Figure 1C). CC5 is unlikely to bind to the surface of XCL1's homodimeric or chemokine structures because XCL1 has a high positive surface charge, as does CC5.[4,14] However, binding could occur during heterodimer formation between monomeric subunits of CC5 and XCL1's β-sheet structure which both have apolar faces that can form the interface of a β-sandwich dimer (Figure 1C). Here, we show by heparin affinity chromatography and NMR that the presence of CC5 indeed modulates the XCL1 structural equilibrium, increasing the population of the β-sheet structure and decreasing the population of the chemokine structure. The increase in the population of the β-sheet structure likely occurs due to sequestration of WT XCL1 in WT XCL1-CC5 heterodimers where both protomers occupy the β-sheet structure. The work presented here lays the groundwork for therapeutically targeting protein metamorphosis in XCL1 and other metamorphic proteins.

2 | MATERIALS AND METHODS

2.1 | Protein expression and purification

XCL1, XCL1 V21C V59C (CC3), XCL1 A36C A49C (CC5), and XCL1 R43A were expressed and purified as previously described.[4,7,23] Briefly, each protein was expressed recombinantly in BL21 DE3 Escherichia coli using pET28a expression vectors. Sequences contained a His6-SUMO tag. Cultures were grown at 37 °C to an optical density of 0.5 to 0.7 in terrific broth with 50 μg/mL kanamycin. Protein expression was then induced by addition of 1 mM isopropyl-b-D-thiogalactopyranoside (IPTG) and cultures were grown for 5 hours at 37 °C. Cells were harvested by centrifugation and stored at −80 °C. Proteins were then purified. Cell pellets were resuspended in 50 mM sodium phosphate (pH 8.0), 300 mM sodium chloride, 10 mM imidazole, 0.1% (v/v) β-mercaptoethanol, and 1 mM phenylmethylsulfonyl fluoride (PMSF). Cells were lysed with a French press. Inclusion bodies were collected from lysates via centrifugation at 12 000g for 20 minutes. Soluble fractions and resuspended inclusion bodies were further purified via Nickel column chromatography. After incubation of soluble and insoluble fractions with Ni^{2+}-NTA resin (Qiagen) for 1 hour at room temperature, columns were rinsed, and proteins were eluted with 6 M guanidinium chloride, 50 mM sodium phosphate (pH 7.4), 300 mM NaCl, 500 mM imidazole, 0.2% sodium azide, and 0.1% (v/v) β-mercaptoethanol. Eluted proteins were then refolded via infinite dilution refolding into 20 mM Tris (pH 8.0), 200 mM NaCl, 10 mM cysteine, and 0.5 mM cystine and incubated at room temperature overnight with gentle stirring. Refolded protein solutions were concentrated to ~50 mL. The His6-SUMO fusion tag was then removed by ULP1 protease cleavage overnight and separated from the protein of interest using cation exchange chromatography on SP Sepharose Fast Flow resin (GE Healthcare UK Ltd.). High performance liquid chromatography with a C18 column was used as a final purification step. Proteins were the frozen and lyophilized. Matrix-assisted

laser desorption ionization time-of-flight (MALDI-TOF) spectroscopy was used to confirm sample purities, identities, and homogeneities.

2.2 | Heparin affinity chromatography

Heparin-sepharose chromatography was used to measure XCL1 GAG binding affinity as previously described.[23–26] In brief, protein samples were prepared in 20 mM phosphate (pH 6.0) and loaded onto a 1 mL HiTrap Heparin HP column (GE Healthcare Life Sciences) attached to an AKTA chromatography system (GE Healthcare Life Sciences). Elution with a linear 0 to 1 M NaCl gradient in 20 mM phosphate (pH 6.0) was monitored by recording the absorbance at 280 nm (in AU, Absorbance Units). For individual protein samples, 400 μg (CC3) or 200 μg (all others) of protein in 1 mL of 20 mM phosphate (pH 6.0) was loaded onto the column. For titrations, 200 μg of XCL1 or XCL1 R43A were mixed with 200 μg CC5 (1:1 samples) or 1000 μg CC5 (5:1 samples) to a total volume of 1 mL in 20 mM phosphate (pH 6.0) and loaded onto the column.

2.3 | 2D ^{15}N-^{1}H heteronuclear single quantum coherence NMR experiments

Lyophilized protein was resuspended in 20 mM sodium phosphate (pH 6.0), 200 mM NaCl, and 10% D2O. Samples were prepared with: (1) 100 μM ^{15}N XCL1 (0:1 CC5:XCL1), (2) 100 μM ^{15}N XCL1 and 50 μM unlabeled CC5 (0.5:1 CC5:XCL1), (3) 100 μM ^{15}N XCL1 and 100 μM unlabeled CC5 (1:1 CC5:XCL1), and (4) 100 μM ^{15}N XCL1 and 500 μM unlabeled CC5 (5:1 CC5:XCL1). Heteronuclear single quantum coherence (HSQC) Spectra were then collected at 40 °C on a Bruker 600 MHz spectrometer and processed with NMRPipe.[27]

2.4 | Calculation of fractional structural occupancy

Intensities of HSQC peaks in the characteristic regions for G44 and W55 were used to estimate relative populations of the two XCL1 conformations, as these peaks are well separated from (a) peaks from other residues and (b) peaks from the same residue in different XCL1 conformations, avoiding any potential interference. Intensities were measured using CARA.[28] For each residue, intensities for the peak from the chemokine fold, β-sheet fold, and third species that appears when XCL1 is exposed to CC5 (likely an XCL1-CC5 heterodimer species) were summed (total intensity; 100%). The intensity of each peak was then divided by this total value as a proxy for the relative population of the structure from which the peak arises.

3 | RESULTS AND DISCUSSION

3.1 | CC5 shifts XCL1's structural equilibrium as measured by heparin affinity chromatography

The XCL1 β-sheet structure binds GAGs such as heparin with much higher affinity than its chemokine structure.[4] Heparin binding can be analyzed by monitoring elution from a heparin-sepharose column. In this assay, XCL1's two structures have distinct elution profiles due to their different heparin affinities, and elution peak volumes can be monitored as a proxy for fractional population of XCL1's different native structures.[24] We thus used

heparin affinity chromatography to assess for changes in relative occupancy of XCL1's structures in response to addition of CC5.

We hypothesized that as increasing concentrations of CC5 were titrated into XCL1, the elution peak from XCL1's chemokine structure would decrease in volume. This would indicate a decrease in the fractional population of the chemokine conformation as the β-sheet structure is stabilized. The elution peak from the β-sheet structure is expected to increase significantly in volume because CC5 elutes at a similar salt concentration as the XCL1 β-sheet structure. Control experiments were performed with CC5, as well as with CC3 which elutes at the same position as the first peak in the XCL1 chromatograph (Figure 2A). We found that titration of one and five equivalents of CC5 into XCL1 caused a dose-dependent decrease in the volume of the first peak in XCL1's heparin affinity chromatograph, indicating that the chemokine fold was depleted in response to CC5 (Figure 2B). This shift, however, was somewhat difficult to detect, because the elution peak from XCL1's chemokine structure is small even in the absence of CC5.

Therefore, we repeated heparin affinity chromatography experiments with an XCL1 variant (XCL1 R43A) with a higher fractional population of the chemokine structure, increasing the intensity of the first elution peak.[24] Notably, this mutation also alters the heparin binding affinity of the β-sheet structure, changing its chromatographic fingerprint (Figure 3). Specifically, the XCL1 R43A chromatograph shows an elution peak from the chemokine structure at ~450 mM NaCl and the β-sheet structure at ~540 mM NaCl (Figure 3). Upon titration of CC5 against XCL1 R43A, both of these peaks decrease in volume (Figure 3). This is likely due to formation of XCL1 R43A-CC5 heterodimers which bind to heparin with higher affinity than XCL1 R43A but lower affinity than CC5, and thus have distinct elution signatures (Figure 3). These results suggest that CC5 depletes the XCL1 R43A chemokine structure. This may occur due to formation of XCL1 R43A-CC5 heterodimers in which both protomers occupy the β-sheet structure.

3.2 | CC5 controls XCL1's metamorphic equilibrium as measured by 2D ^{15}N-^{1}H HSQC experiments

Changes in XCL1's conformational equilibrium can be measured in more detail using 2D ^{1}H-^{15}N NMR HSQC experiments. XCL1's distinct structures have different HSQC fingerprints[6] (Figure S1A), and HSQC peak intensities can be used to quantify the relative population of the two XCL1 structures. Using HSQC experiments, we monitored changes in ^{15}N XCL1's fractional structural population in response to addition of unlabeled CC5. We found that upon titration of increasing quantities of CC5 into XCL1, the HSQC peaks from the XCL1 chemokine fold decrease in intensity and eventually disappear (Figures 4 and S1). Peaks from the β-sheet structure intensify, and in some cases, new peaks adjacent to the β-sheet peaks appear and intensify (Figures 4 and S1). This is particularly visible in a known diagnostic region for XCL1's folded conformation,[4] shown in Figure 4A, where a new peak for A49 appears adjacent to the A49 peak from the XCL1 β-sheet structure and intensifies in response to titration of increasing concentrations of CC5). Similar transitions occur for the signals for G44 and the W55 indole NH, previously identified as diagnostic reporters of XCL1's metamorphic equilibrium (Figure 4B). We tentatively assigned the new

peaks to a XCL1-CC5 heterodimeric species, where both protomers are in the β-sheet fold, and in which these residues occupy similar, but detectably distinct, chemical environments.

Next, we quantified fractional populations of the two XCL1 structures. Certain reporter residues are particularly well suited for this purpose because their HSQC peaks are well resolved from one another as well as from other peaks. One such reporter residue is Glycine 44, which is located in a loop in XCL1's chemokine fold and a β-strand in XCL1's β-sheet fold (Figure 1A). A second reporter peak arises from the indole NH of XCL1's sole tryptophan, W55. In the chemokine fold, W55 is located in the α-helix, whereas in the β-sheet structure, W55 is in a disordered region (Figure 1A). We calculated peak intensities for both G44 and W55 after addition of 0, 0.5, 1, and 5 equivalents of CC5 to XCL1, and used peak intensities as a proxy for fractional occupancy of XCL1's structures (Figure 4B). We found that the chemokine fold decreases from >50% occupancy to <40% occupancy after addition of 1 equivalent of CC5, and finally to <5% occupancy after addition of 5 equivalents of CC5 (Figure 4C). The population of WT XCL1 β-sheet homodimers also decreases in response to addition of CC5. The fractional intensity of the new peaks adjacent to the β-sheet peaks increases from ~35% after addition of 0.5 equivalents of CC5 to nearly 80% after addition of 5 equivalents (Figure 4C). Together, this data supports the hypothesis that CC5 enriches XCL1's β-sheet conformation and depletes its chemokine conformation, likely by forming stable XCL1-CC5 heterodimers in which both protomers are in the β-sheet conformation. As such, the population of WT XCL1 β-sheet structure homodimers is also reduced.

4 | CONCLUSIONS

XCL1 is a metamorphic protein with two distinct native states that have different biologic functions. In this work, we show by heparin affinity chromatography and 2D NMR that an engineered XCL1 variant called CC5 can modulate the relative population of the two XCL1 structures. We propose that CC5 does this by forming stable heterodimers with XCL1's β-sheet structure, in which both protomers occupy the β-sheet structure. CC5 can be used going forward as a molecular tool by which to regulate XCL1's dynamic interconversion, allowing for studies that further elucidate the biologic roles of XCL1 metamorphosis, for example, in fighting infection and cancer.

Demonstrating that XCL1 interconversion can be controlled by titration of an exogenous molecule lays the groundwork for drugging XCL1 by shifting its structural equilibrium with traditional drug-like molecules. This could occur via selective binding and stabilization of the monomeric chemokine structure or by acting as a chemical inducer of dimerization that promotes a shift to the all-beta structure analogous to the CC5-induced effects observed in this study. Examples of well-characterized chemical inducers of dimerization can bind their targets with low nanomolar affinity and induce dimerization even when the inherent propensity for dimerization in the absence of drug is low. For example, FK506 (aka Tacrolimus) is a sub-nanomolar FKBP ligand that induces dimerization with calcineurin.[29] Another chemical inducer of dimerization, mandipropamid, induces dimerization between the plant ABA receptor PYR1 and PP2C HAB1 thus inhibiting PP2C activity with an EC50 in the low nanomolar range.[30] Therefore, we can envision a chemical inducer of

dimerization for XCL1 which is effective at nanomolar concentrations. XCL1 is known to be secreted by activated T Cells in nanogram quantities.[31] To reach saturating concentrations of a chemical inducer of dimerization with a low nanomolar affinity for XCL1 would require likely ligand concentrations in target tissues in the nanomolar to micromolar ranges which are commonly achieved with small molecule drugs.

Additionally, a new variant of XCL1 could be designed, which is locked in the β-sheet structure but selectively heterodimerizes with WT XCL1. Theoretically, the residues making up the core of the CC5 dimer could be repacked to discourage CC5 dimerization and enhance WT XCL1-CC5 heterodimerization. However, this would likely only be accomplished after significant design and screening efforts. A conceptually simpler approach would be to append a domain to the CC5 C-terminus that selectively binds to the WT XCL1 C-terminus, driving up local concentrations of the new locked variant in proximity to WT XCL1 and facilitating heterodimerization.

More broadly, controlling XCL1's metamorphic interconversion demonstrates the principle that protein metamorphosis can be drugged, illuminating a novel therapeutic mechanism with numerous potential advantages. Depleting rather than inhibiting a pathogenic molecule has recently emerged as a promising, unconventional therapeutic strategy with several advantages over the classical model of binding and inhibiting target molecules. For example, Proteolysis-targeting chimeras (PROTACs) are drugs that hijack the E3 ubiquitin ligase system to mediate proteasomal degradation of a pathogenic target protein.[32–34] PROTACs have been shown to act with high stringency and can be used to target proteins that might otherwise have been considered "un-druggable."[32–34] Therapies that target metamorphosis offer similar advantages by mechanistically employing the same "depletion not inhibition" strategy used by PROTACs. Drugs targeting metamorphosis would essentially delete the pathogenic conformation of a metamorphic protein by converting the drug-bound target molecule to a functionally inert structure. However, drugs that alter a protein's metamorphic equilibrium will bring additional advantages such as reversibility and independence from cellular machinery. While reversing the effect of a PROTAC requires synthesis of new target protein, drugs that target metamorphosis would act reversibly because the target protein's structural equilibrium would return to normal after the drug is eliminated. Additionally, drugs targeting metamorphosis will not rely on additional cellular machinery to carry out their effects, vs PROTACs which require the E3 ubiquitin ligase system and proteasomal degradation system in order to execute their function.[32–34] Finally, in a case where a metamorphic protein's multiple structures carry out multiple biologic functions, depleting only the pathogenic structure would allow for the other structure to persist and continue to execute its physiologic role.

While fewer than 100 metamorphic proteins have been identified to date, it is estimated that metamorphic proteins make up as much as 4% of the PDB.[3] Moreover, known metamorphic proteins are involved in critical biologic processes such as cell cycle regulation,[35,36] circadian rhythms,[37] and transcription/translation,[22] as well as disease processes such as cancer.[38–58] As increasing numbers of metamorphic proteins are discovered with diverse roles in human health and disease,[3] therapeutically targeting protein metamorphosis is emerging as a unique, attractive option for blocking or altering

protein function.[2,59] The work presented here lays the foundation for efforts toward such therapies.

Supplementary Material

Refer to Web version on PubMed Central for supplementary material.

ACKNOWLEDGMENTS

This work was supported in part by a grant from the State of Wisconsin Tax Check-Off Program for Cancer Research and the Medical College of Wisconsin Cancer Center as well as NIH grants R01 AI058072, S10 OD020000, S10 OD025000 (to Brian F. Volkman), and F30 CA236182 (to Acacia F. Dishman). Acacia F. Dishman is a member of the NIH supported (T32 GM080202) Medical Scientist Training Program at the Medical College of Wisconsin.

Funding information

National Institutes of Health, Grant/Award Numbers: T32 GM080202, F30 CA236182, S10 OD025000, S10 OD020000, R01 AI058072

REFERENCES

[1]. Murzin AG, Science 2008, 320, 1725. [PubMed: 18583598]

[2]. Dishman AF, Volkman BF, ACS Chem. Biol 2018, 13, 1438. [PubMed: 29787234]

[3]. Porter LL, Looger LL, Proc. Natl. Acad. Sci. U. S. A 2018, 115, 5968. [PubMed: 29784778]

[4]. Tuinstra RL, Peterson FC, Kutlesa S, Elgin ES, Kron MA, Volkman BF, Proc. Natl. Acad. Sci. U. S. A 2008, 105, 5057. [PubMed: 18364395]

[5]. Kuloglu ES, McCaslin DR, Kitabwalla M, Pauza CD, Markley JL, Volkman BF, Biochemistry 2001, 40, 12486. [PubMed: 11601972]

[6]. Kuloglu ES, McCaslin DR, Markley JL, Volkman BF, J. Biol. Chem 2002, 277, 17863. [PubMed: 11889129]

[7]. Nevins AM, Subramanian A, Tapia JL, Delgado DP, Tyler RC, Jensen DR, Ouellette AJ, Volkman BF, Biochemistry 2016, 55, 3784. [PubMed: 27305837]

[8]. Dishman AF, Lee MW, de Anda J, Lee EY, He J, Huppler AR, Wong GCL, Volkman BF, ACS. Infect. Dis 2020, 6, 1204. [PubMed: 32243126]

[9]. Crozat K, Guiton R, Contreras V, Feuillet V, Dutertre CA, Ventre E, Vu Manh TP, Baranek T, Storset AK, Marvel J, Boudinot P, Hosmalin A, Schwartz-Cornil I, Dalod M, J. Exp. Med 2010, 207, 1283. [PubMed: 20479118]

[10]. Lei Y, Takahama Y, Microbes Infect. 2012, 14, 262. [PubMed: 22100876]

[11]. Dorner BG, Dorner MB, Zhou X, Opitz C, Mora A, Guttler S, Hutloff A, Mages HW, Ranke K, Schaefer M, Jack RS, Henn V, Kroczek RA, Immunity 2009, 31, 823. [PubMed: 19913446]

[12]. Lei Y, Ripen AM, Ishimaru N, Ohigashi I, Nagasawa T, Jeker LT, Bosl MR, Hollander GA, Hayashi Y, Malefyt Rde W, Nitta T, Takahama Y, J. Exp. Med 2011, 208, 383. [PubMed: 21300913]

[13]. Guzzo C, Fox J, Lin Y, Miao H, Cimbro R, Volkman BF, Fauci AS, Lusso P, PLoS Pathog. 2013, 9, e1003852. [PubMed: 24385911]

[14]. Fox JC, Tyler RC, Guzzo C, Tuinstra RL, Peterson FC, Lusso P, Volkman BF, ACS Chem. Biol 2015, 10, 2580. [PubMed: 26302421]

[15]. Guzzo C, Fox JC, Miao H, Volkman BF, Lusso P, J. Virol 2015, 89, 9061. [PubMed: 26085164]

[16]. Mony JT, Schuchert MJ, Front. Immunol 2018, 9, 2298. [PubMed: 30374348]

[17]. Chou WC, Hsiung CN, Chen WT, Tseng LM, Wang HC, Chu HW, Hou MF, Yu JC, Shen CY, Int. J. Cancer 2020, 146, 2182. [PubMed: 31904872]

[18]. Yang XL, Qi LG, Lin FJ, Ou ZL, Breast Cancer (Dove Med Press) 2017, 9, 227. [PubMed: 28408852]

[19]. Keen JC, Garrett-Mayer E, Pettit C, Mack KM, Manning J, Herman JG, Davidson NE, Cancer Biol. Ther 2004, 3, 1304. [PubMed: 15662126]

[20]. Tuinstra RL, Peterson FC, Elgin ES, Pelzek AJ, Volkman BF, Biochemistry 2007, 46, 2564. [PubMed: 17302442]

[21]. Lopez-Pelegrin M, Cerda-Costa N, Cintas-Pedrola A, Herranz-Trillo F, Bernado P, Peinado JR, Arolas JL, Gomis-Ruth FX, Angew. Chem. Int. Ed. Engl 2014, 53, 10624. [PubMed: 25159620]

[22]. Burmann BM, Knauer SH, Sevostyanova A, Schweimer K, Mooney RA, Landick R, Artsimovitch I, Rosch P, Cell 2012, 150, 291. [PubMed: 22817892]

[23]. Fox JC, Nakayama T, Tyler RC, Sander TL, Yoshie O, Volkman BF, Cytokine+ 2015, 71, 302. [PubMed: 25497737]

[24]. Volkman BF, Liu TY, Peterson FC, Chapter 3 Lymphotactin Structural Dynamics. in Chemokines, Part B, Elsevier, Amsterdam 2009, p. 51.

[25]. Fox JC, Tyler RC, Peterson FC, Dyer DP, Zhang F, Linhardt RJ, Handel TM, Volkman BF, Biochemistry 2016, 55, 1214. [PubMed: 26836755]

[26]. Handel TM, Johnson Z, Crown SE, Lau EK, Proudfoot AE, Annu. Rev. Biochem 2005, 74, 385. [PubMed: 15952892]

[27]. Delaglio F, Grzesiek S, Vuister GW, Zhu G, Pfeifer J, Bax A, Biomol J. NMR 1995, 6, 277.

[28]. Keller R. Computer-aided resonance assignment (CARA). http://cara.nmr.ch/doku.php.

[29]. Bierer BE, Mattila PS, Standaert RF, Herzenberg LA, Burakoff SJ, Crabtree G, Schreiber SL, Proc. Natl. Acad. Sci. U. S. A 1990, 87, 9231. [PubMed: 2123553]

[30]. Park SY, Peterson FC, Mosquna A, Yao J, Volkman BF, Cutler SR, Nature 2015, 520, 545. [PubMed: 25652827]

[31]. Tikhonov I, Kitabwalla M, Wallace M, Malkovsky M, Volkman B, Pauza CD, Cytokine+ 2001, 16(), 73. [PubMed: 11683588]

[32]. Churcher I, J. Med. Chem 2018, 61, 444. [PubMed: 29144739]

[33]. Bondeson DP, Smith BE, Burslem GM, Buhimschi AD, Hines J, Jaime-Figueroa S, Wang J, Hamman BD, Ishchenko A, Crews CM, Cell Chem. Biol 2018, 25, 78 e5. [PubMed: 29129718]

[34]. Paiva SL, Crews CM, Curr. Opin. Chem. Biol 2019, 50, 111. [PubMed: 31004963]

[35]. Luo X, Tang Z, Xia G, Wassmann K, Matsumoto T, Rizo J, Yu H, Nat. Struct. Mol. Biol 2004, 11, 338. [PubMed: 15024386]

[36]. Valenzuela SM, Mazzanti M, Tonini R, Qiu MR, Warton K, Musgrove EA, Campbell TJ, Breit SN, J. Physiol 2000, 529, 541. [PubMed: 11195932]

[37]. Chang YG, Cohen SE, Phong C, Myers WK, Kim YI, Tseng R, Lin J, Zhang L, Boyd JS, Lee Y, Kang S, Lee D, Li S, Britt RD, Rust MJ, Golden SS, LiWang A, Science 2015, 349, 324. [PubMed: 26113641]

[38]. Li BP, Mao YT, Wang Z, Chen YY, Wang Y, Zhai CY, Shi B, Liu SY, Liu JL, Chen JQ, Cell. Physiol. Biochem 2018, 46, 907. [PubMed: 29669336]

[39]. Zhao K, Wang Z, Li X, Liu JL, Tian L, Chen JQ, Mol. Cell. Biochem 2019, 462, 97. [PubMed: 31473882]

[40]. Chen CD, Wang CS, Huang YH, Chien KY, Liang Y, Chen WJ, Lin KH, Proteomics 2007, 7, 155. [PubMed: 17154271]

[41]. Peretti M, Angelini M, Savalli N, Florio T, Yuspa SH, Mazzanti M, Biochim. Biophys. Acta 2015, 1848, 2523. [PubMed: 25546839]

[42]. Lu J, Dong Q, Zhang B, Wang X, Ye B, Zhang F, Song X, Gao G, Mu J, Wang Z, Ma F, Gu J, Med Oncol 2015, 32, 616. [PubMed: 25920608]

[43]. Ye Y, Yin M, Huang B, Wang Y, Li X, Lou G, Tumour Biol 2015, 36, 4175. [PubMed: 25582317]

[44]. Singha B, Harper SL, Goldman AR, Bitler BG, Aird KM, Borowsky ME, Cadungog MG, Liu Q, Zhang R, Jean S, Drapkin R, Speicher DW, Sci. Rep 2018, 8, 14725. [PubMed: 30282979]

[45]. Ding Q, Li M, Wu X, Zhang L, Wu W, Ding Q, Weng H, Wang X, Liu Y, Tumour Biol 2015, 36(), 193. [PubMed: 25227665]

[46]. He YM, Zhang ZL, Liu QY, Xiao YS, Wei L, Xi C, Nan X, J Cell Mol Med 2018, 22, 2569. [PubMed: 29516682]

[47]. Yu W, Cui R, Qu H, Liu C, Deng H, Zhang Z, Exp Ther Med 2018, 15, 4943. [PubMed: 29805518]

[48]. Petrova DT, Asif AR, Armstrong VW, Dimova I, Toshev S, Yaramov N, Oellerich M, Toncheva D, Clin. Biochem 2008, 41, 1224. [PubMed: 18710659]

[49]. Wang P, Zhang C, Yu P, Tang B, Liu T, Cui H, Xu J, Mol. Cell. Biochem 2012, 365, 313. [PubMed: 22426742]

[50]. Byrne T, Coleman HG, Cooper JA, McCluggage WG, McCann A, Furlong F, Oncotarget 2017, 8, 102223. [PubMed: 29254238]

[51]. Teixeira JH, Silva P, Faria J, Ferreira I, Duarte P, Delgado ML, Queiros O, Moreira R, Barbosa J, Lopes CA, do Amaral JB, Monteiro LS, Bousbaa H, Oral. Dis 2015, 21, 713. [PubMed: 25754611]

[52]. Li L, Xu DB, Zhao XL, Hao TY, Arch. Gynecol. Obstet 2013, 288, 155. [PubMed: 23334889]

[53]. Schuyler SC, Wu YF, Kuan VJ, J. Cell Sci 2012, 125, 4197. [PubMed: 23093575]

[54]. Iimori M, Kitao H, Maehara Y, Cell Cycle 2015, 14, 946. [PubMed: 25803575]

[55]. Li GQ, Zhang HF, World J Gastroenterol 2004, 10, 3218. [PubMed: 15457580]

[56]. Kato T, Daigo Y, Aragaki M, Ishikawa K, Sato M, Kondo S, Kaji M, Lung Cancer 2011, 74, 124. [PubMed: 21376419]

[57]. Wang X, Jin DY, Ng RW, Feng H, Wong YC, Cheung AL, Tsao SW, Cancer Res. 2002, 62, 1662. [PubMed: 11912137]

[58]. Bates M, Furlong F, Gallagher MF, Spillane CD, McCann A, O'Toole S, O'Leary JJ, Cancer Lett. 2020, 469, 11. [PubMed: 31593803]

[59]. Zamora-Carreras H, Maestro B, Sanz JM, Jimenez MA, ChemBioChem 2020, 21, 432. [PubMed: 31456307]

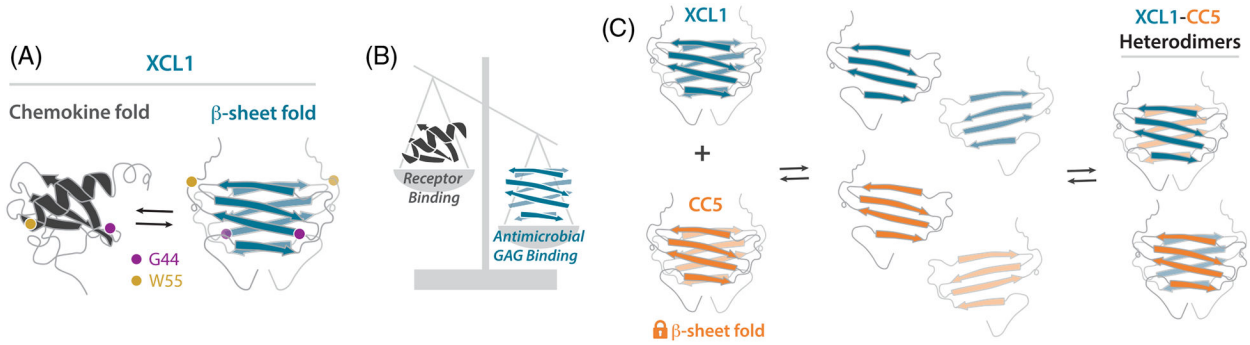

FIGURE 1.

Model for tuning XCL1's metamorphic equilibrium. A, The two XCL1 native structures. Chemokine structure (monomer): dark gray, left. β-sheet structure (dimer): subunit A, dark teal/subunit B, light teal. Reporter residues G44 (purple) and W55 (gold) are highlighted. B, Shifting the relative population of XCL1 structures could alter XCL1 function. The chemokine structure is responsible for receptor binding, while the β-sheet structure is responsible for GAG binding and antimicrobial activity. C, Schematic of a possible mechanism by which CC5 could control XCL1's structural equilibrium via the formation of stable XCL1-CC5 heterodimers. CC5 (dimer): subunit A, dark orange/subunit B, light orange; XCL1 β-sheet fold (dimer): subunit A, dark teal/subunit B, light teal

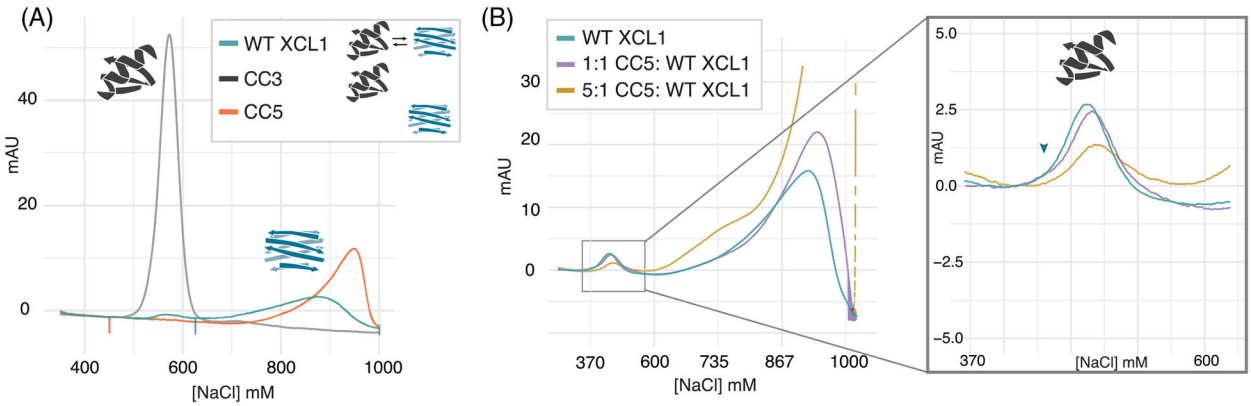

FIGURE 2.

A, Heparin column chromatographs for an engineered, locked chemokine fold variant of XCL1 (CC3), a locked β-sheet fold variant of XCL1 (CC5), and XCL1. B, Heparin column chromatographs for XCL1 alone and after addition of 1 and 5 equivalents of CC5. The peak from the chemokine structure decreases in volume as more CC5 is added

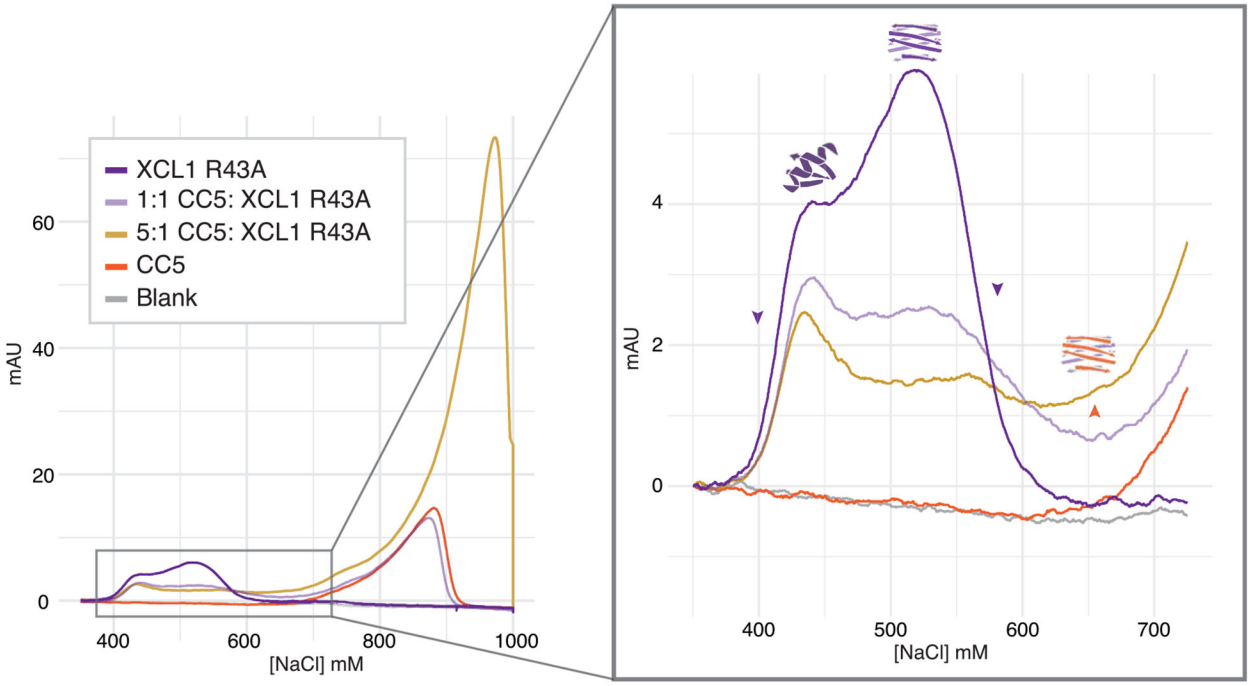

FIGURE 3.

Heparin affinity chromatography during titration of CC5 against XCL1 R43A. The XCL1 R43A chromatograph shows a peak from the chemokine structure that elutes at ~450 mM NaCl, and a peak from the β-sheet structure that elutes at ~540 mM NaCl. As CC5 is titrated against XCL1 R43A, both peaks decrease in volume

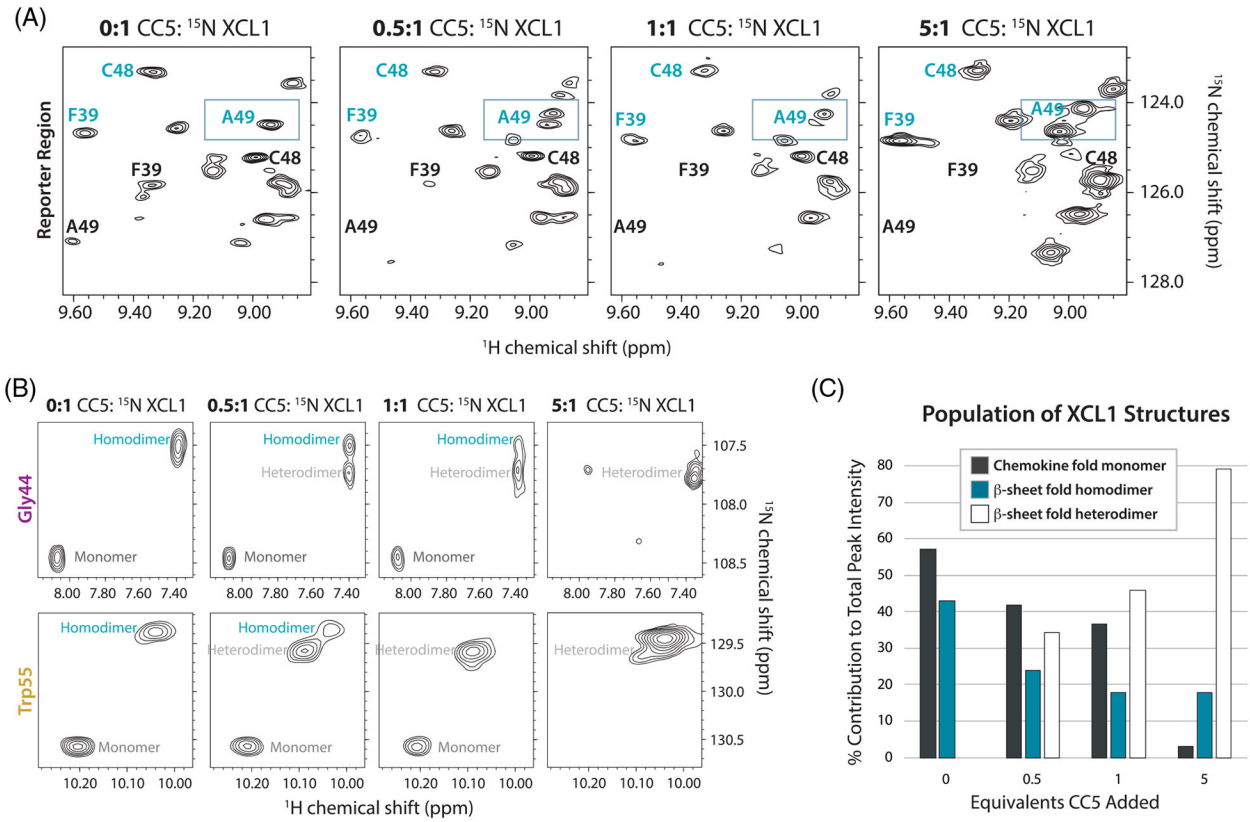

FIGURE 4.

A, A diagnostic region of the XCL1 HSQC spectrum with peaks from the chemokine fold labeled in dark gray and peaks from the β-sheet fold labeled in teal. A49, highlighted in a teal box, shows the appearance of a second peak adjacent to the peak from the β-sheet fold, likely from an XCL1-CC5 heterodimeric species. B, HSQC spectra zoomed in on the G44 (top) and W55 (bottom) reporters during titration of unlabeled CC5 against ^{15}N XCL1. Conditions for A and B: 40 °C, 200 mM NaCl, pH 6.0, 100 μM XCL1. C, Relative population of XCL1 structures, as measured by % contribution to total peak intensities (values calculated for G44 and W55 reporters, then averaged)